物理与工程　Vol.35　No.4　2025

GENERALIZED FIBONACCI ZONE PLATE

LI Baoping[1]　CHEN Jian[2]　WANG Jing[1]

([1] Tianjin Science and Technology Museum, Tianjin 300210; [2] Tianjin Yaohua High School, Tianjin 300000)

Abstract　Zone plates play an important role in X-ray and optics fileds. In this work, we proposed a generalized Fibonacci zone plates (GFiZP) is proposed, which enables the manipulation of focusing properties for X-ray and light. Compared to conventional Fibonacci zone plates (FiZPs) and Cantor-type fractal zone plates (FraZPs), this device offers additional degrees of freedom for engineering focusing performance. In comparison with FraZPs, GFiZPs are constructed with inflation rule instead of extraction rule, thus avoiding sparse structures at high recursion orders, the sparse structures would lead to issues in fabrication. Notably, numerical simulations demonstrate that, similar to FraZPs, GFiZPs retain two critical functionalities: multi-focal capability and self-similar intensity distribution. Furthermore, we conducted a detailed investigation into the axial irradiance profiles of GFiZPs with varying structural parameters. Given these favorable properties, this novel zone plate design holds great potential for expanded applications in areas such as optical manufacturing and optical manipulation of microparticles.

Key words　zone plate; Fibonacci series; focusing points manipulation; fractal self-similarity

扩展斐波那契波带片

李保平[1]　陈　健[2]　王　静[1]

([1] 天津科学技术馆,天津　300210;[2] 天津市耀华中学,天津　300000)

摘　要　波带片在X射线与光学领域中发挥着重要作用。本文提出了一种广义斐波那契波带片(generalized Fibonacci zone plate, GFiZP)设计,该设计能够实现对X射线与光线聚焦特性的调控。与传统斐波那契波带片(Fibonacci zone plate, FiZP)及康托型分形波带片(Cantor-type fractal zone plate, FraZP)相比,该器件为调控聚焦性能提供了更多自由度。相较于康托型分形波带片,广义斐波那契波带片采用膨胀规则而非提取规则构建而成,因此可避免在高递归阶数下形成稀疏结构——而这类稀疏结构往往会给制备工艺带来难题。值得注意的是,数值模拟结果表明,与康托型分形波带片类似,广义斐波那契波带片同样具备两项关键功能:多焦点特性与自相似强度分布。此外,本文还针对不同结构参数下广义斐波那契波带片的轴向辐照度分布展开了详细研究。凭借这些优良特性,这种新型波带片设计在光学制造、微粒子光学操控等领域具有广阔的拓展应用前景。

关键词　波带片; 斐波那契数列; 焦点调控;分形自相似

Received: 2024-08-05

Corresponding Author: WANG Jing, wangjingkjg@163.com。

Cite this article: LI B P, CHEN J, WANG J. Generalized Fibonacci zone plate[J]. Physics and Engineering, 2025, 35(4): 305-309, 318.

The interest in zone plates has been re-inspired recently due to their imaging and focusing capabilities in THz and soft X-ray regimes[1-2]. Unlike conventional refractive optics, which suffer from severe absorption issues in these spectral ranges, zone plates—operating on the principle of diffraction—effectively address this technical bottleneck. To optimize the focusing and imaging performance of zone plates, numerous innovative designs have been reported, such as modified Fresnel zone plates[3] and Cantor-type fractal zone plates (FraZPs)[4-6]. Among these designs, FraZPs have garnered significant attention due to their unique on-axis self-similar intensity distribution. Distinct from conventional Fresnel zone plates (FZPs)—which consist of alternating transparent and opaque circular rings with uniform width along the squared radial coordinate—FraZPs are characterized by a fractal profile along the squared radial coordinate. To date, extensive theoretical and experimental studies have been conducted to explore the fundamental properties of FraZPs[4,7-13], while their practical applications have also been successfully demonstrated[14-15]. Among them, Cantor-type ones are the most common fractal structures to construct the fractal diffractive optical elements, and amazing properties of Cantor-like FraZPs, such as finely tunable foci[14], reduced chromatic aberration in white imaging[15], etc. have been observed. However, due to the intrinsic features of the Cantor-sets, sparse structures will be inevitably generated at a large number of iterations, hence leading to issues of fabricating and limiting their applications for high-resolution imaging or focusing. To avoid the sparse structures without losing the fractal properties, alternative solutions are highly desired. Fibonacci inflation rule could be one of excellent candidate for this issue. This rule has been used to study the quasi-periodic systems comprehensively[16-17].

We have reported the Fibonacci zone plates (FiZPs)[18] by squeezing the circular Fibonacci grating[19] into the squared radial coordinate. Experimental and numerical results showed that similar to FZPs and FraZPs, FiZPs could form multiple foci on the optical axis. In this letter, we further present generalized Fibonacci zone plates (GFiZPs) as a new family of diffractive lenses, whose structure is basically a generalized Fibonacci sequence[20] within the framework of square radial coordinate. Generally, GFiZPs own more construction parameters to engineer the axial response in comparison with the conventional FiZPs (only a particular case of GFiZPs). Theoretical analysis shows GFiZPs possess multiple foci along the optical axis and internal fractal properties in the on-axis intensity distribution. Meanwhile, the structures with higher recursion can be easily constructed by just extending the external belts according to the Fibonacci inflation rule, thus avoiding the sparse structures generated by the extracting rules for Cantor-sets. Moreover, we have additional freedom to engineer GFiZPs so as to optimize the focusing properties by controlling the ratio of widths (RW) between the two elementary bars.

The generation rule of generalized Fibonacci lattices is introduced first. Let's define A as the initiator (stage S=0). Then at successive operations, the following substitution rules are applied, A→B, B→$B^n A^m$, here n and m are positive integers and A^m represents a string of m A's. Another definition can be provided by the inflation rule $S_{l+1}=S_l^n S_{l-1}^m$, where S_l is the l^{th} generational sequence. Higher recursions can be obtained by repeated inflation. The generalized Fibonacci series characterized by value of (n,m) for $(n,m)=(1,1),(2,1),(3,1),(1,2),(1,3)$ and $(2,2)$ are conventionally called golden, silver, bronze, copper, nickel, and mixed mean, respectively[14]. It is obvious that the conventional Fibonacci lattices here correspond to the golden mean lattice with RW$=(\sqrt{5}-1)/2$. After introducing the n and m, more parameters can be tuned to generate the fractal zone plate, which can enable diverse applications. And with this rule, the zone plate can be constructed with a inflation method instead of extraction rules. As an example, Fig. 1(a) shows the first four stages of the silver mean Fibonacci lattice with $n=2$, $m=1$. Here, A and B are the elementary bars with given lengths of L_a and L_b respectively. For comparison, Fig. 1(b) shows the Cantor-sets generated by the extraction rule. We can clearly see that Fibonacci lattices generated by the inflation rule can effectively avoid the sparse structures in Cantor-sets generated by the extraction rule, especially for higher recursions.

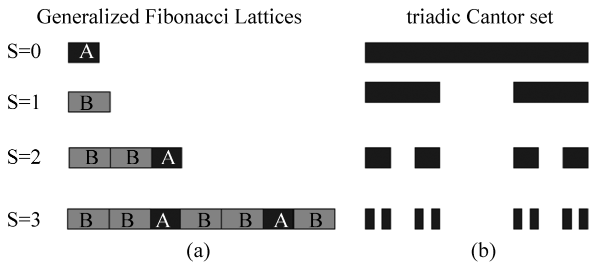

Fig. 1 (Color online) Schemetics for silver Fibonacci lattices (a) and the Cantor-sets (b) generated by the inflation and extraction rules, respectively

GFiZPs are therefore generated by rotating the generalized Fibonacci lattices as in Fig. 1(a) around one extreme and then transforming from the squared radial coordinate to the radial coordinate. Figures 2(a)～(f) show six GFiZPs corresponding to six generalized Fibonacci lattices with the recursion order $S=5$.

To explore the on-axis intensity distribution of GFiZPs, Fresnel approximation is adopted similar to Ref. [4], the intensity along the axis can be expressed as

$$I(0,0,z)=\left(\frac{2\pi}{\lambda z}\right)^2\left|\int_0^a T(r_0^2)\exp\left(-i\frac{\pi}{\lambda z}r_0^2\right)r_0\,\mathrm{d}r_0\right|^2 \tag{1}$$

where a is the maximum extent of the pupil function and l is the wavelength of the incident light. A new variable was defined to transform the coordinate into square radial framework, as $\zeta=r_0^2$. Thus $q(\zeta)=T(r_0)$, here $q(\zeta)$ is just the

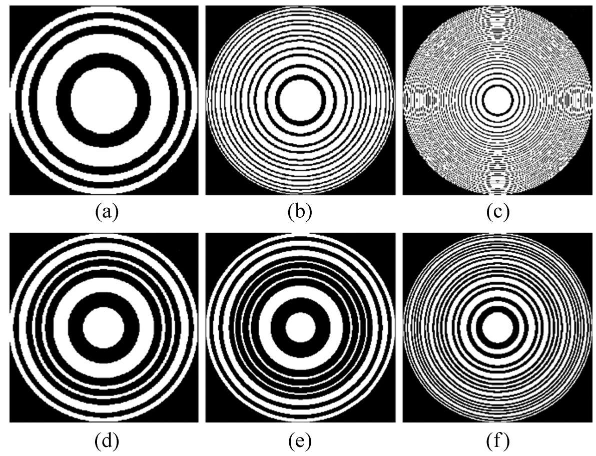

Fig. 2 The GFiZPs generated from (a) golden, (b) silver, (c) bronze, (d) copper, (e) nickel, and (f) mixed mean lattices, respectively. In all cases $S=5$ and RW=1. The patterns have been rescaled individually to match the publishing

transmittance function of generalized Fibonacci lattices. To simplify the formula further, reduced axial coordinate was used as $u=1/\lambda z$. Therefore, the irradiance along the optical axis can be expressed as:

$$I_0(u)=4\pi^2u^2\left|\int_0^{a^2}q(\zeta)\exp(-i2\pi u\zeta)\,\mathrm{d}\zeta\right|^2 \tag{2}$$

Considering the zero transmittance outside the pupil, the on-axis intensity distribution of GFiZPs can be expressed as the Fourier transform of the structure formed in Fig. 1,

$$I_0(u)=4\pi^2u^2\,|F\{q(\zeta)\}|^2 \tag{3}$$

where $F\{q(\zeta)\}$ represents the Fourier transform of $q(\zeta)$. Inasmuch the axial irradiance is expressed in terms of Fourier transform of generalized Fibonacci sequence, it is straightforward to conclude that the on-axis intensity would show the fractal features, which inherits from the Fibonacci sequences.

As aforementioned, the Fourier amplitudes of Fibonacci lattices render the axis behavior of the GFiZPs and thus can be evaluated by the recursion relation as

$$G_{l+1}(u)=\sum_{j=0}^{n-1}e^{2\pi iju F_l}G_l(u)+\sum_{j=0}^{m-1}e^{2\pi iu(nF_l+jF_{l-1})}G_{l-1}(u) \tag{4}$$

where i is imaginary unit, l is the recursion order and $G_l(u)$ denotes the Fourier transform of $q(\zeta)$, F_l represents the width of the l^{th} Fibonacci lattice. Figures 3(a)～(h) show the axial irradiances of the bronze mean lattices ($n=3$, $m=1$, RW$=1$) and nickel mean lattices ($n=1$, $m=3$, RW$=1$) with increasing recursion order from 5 to 8. It can be seen that the axial positions of the main lobes of foci are invariant with different recursion orders. And intensity profiles of higher recursion orders are similar to those of the lower recursion orders, i. e. the self-similarity property inheriting from the Fibonacci lattices. Because the construction rule of GFiZPs is inflation instead of extraction or squeezing, the self-similarity property of GFiZPs differs from that of the Cantor-like FraZPs, whose axial coordinates have to be magnified to observe the self-similarity.

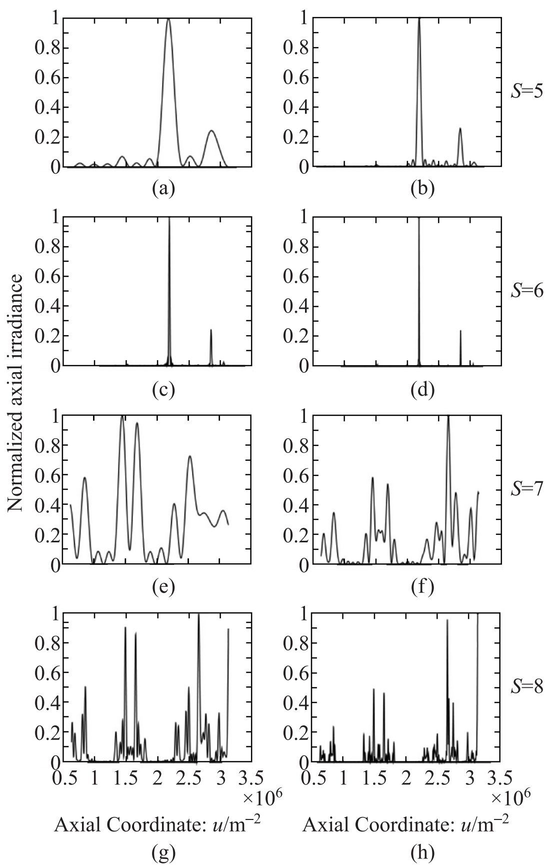

Fig. 3 The on-axis intensity distributions of GFiZPs with four recursion orders for bronze mean lattice ($n=3$, $m=1$, RW$=1$, left column) and nickel mean lattice ($n=1$, $m=3$, RW$=1$, right column). The incident wavelength is set as 532 nm in all figures

To explore the detailed axial irradiance properties of GFiZPs, twist plots are adopted, which are achieved by sequentially stacking the on-axis intensity profiles computed with various RW. Figures 4(a)～(f) show the twist plots computed with the RW ranging from 0. 4 to 2. One can see that the multi-foci profile will become simple with increasing n while $m=1$ (Refer to Figs. 4(a)～(c)). This tendency ascribes to the generated Fibonacci lattices, which is similar to rectangular grating with duty cycle larger than 1 as large n was adopted. The behavior of GFiZP with large n value is thus like a Fresnel zone plate (Refer to Figs. 2(b) and (c)), as the corresponding lattice of FZPs in square radial coordinate is just the rectangular grating. Contrary to the case of $n>1$, when $m>1$ and $n=1$, the on-axis behaviors of GFiZPs become complicated. As shown in Figs. 4(a), (d) and (e), the patterns of their twist plots are very similar but squeezing more lobes into the plots with increased m, because

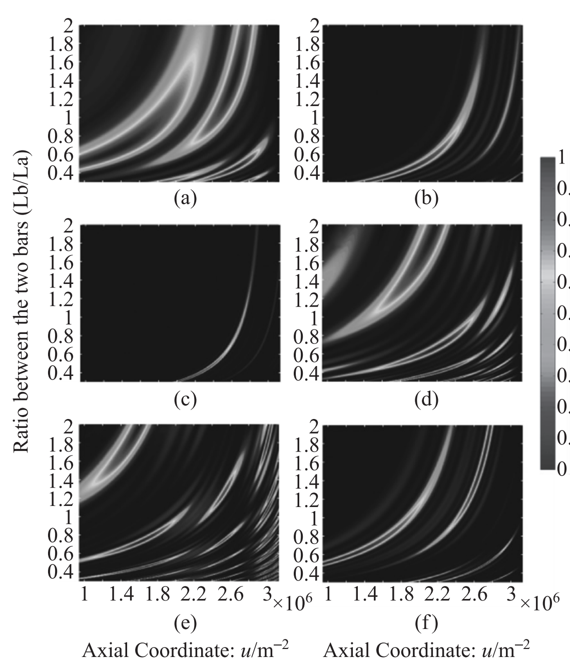

Fig. 4 (Color online) The axial irradiances given by GFiZPs with golden (a), silver (b), bronze (c), copper (d), nickel (e), and mixed (f) mean lattices, respectively. Note the intensity is normalized individually in each plot

the large m value diminishes the duty cycle of generalized Fibonacci lattices. This behavior can also be concluded from Figs. 2(d) and (e), in which their patterns are very similar but more belts are added outside in Fig. 2(e). Finally, when $n=2$ and $m=2$, the twist plot is almost the same as the case of golden mean lattice ($n=1$ and $m=1$) except the decreased focal depths. This is understood readily with the same recursion rule but large gap width.

For the conventional Fibonacci lattice, widths of A and B parts (refer to Fig. 1(a)) are set as golden ratio, i. e. $L_b/L_a=(\sqrt{5}-1)/2$. From the viewpoint of conventional FZPs, the axial irradiance behavior of zone plates can be interpreted as the interference between the successive belts over the pupil. The RW, which relates to the width of transparent rings, thus affects the focusing properties of GFiZPs. From Figs. 4(b) and (c), one can see that the number of foci keeps constant when $n>1$ and $m=1$ while locations of foci change with various RWs. However, for the case of $m>1$ and $n=1$, both the number and location of foci vary with different RW values (see Figs. 4(d) and (e)). For the case of $m=n$, the behavior of GFiZPs falls in between the above two situations. For Figs. 4(a) and (f), the twist plot can be split into two parts by the line of RW=1, one (RW<1) is like Figs. 4(b) and (c), the other (RW>1) is like Figs. 4(d) and (e). The FWHM (Full Width at Half Maximum) is an important property of focal points. However, the FWHM can only be achieved with Fresnel diffraction simulation-this is out of the method of this paper, and we will discuss this feature further.

In conclusion, a new family of zone plates, so-called a generalized Fibonacci zone plate (GFiZP), is proposed. In comparison with Cantor-type FraZPs, GFiZPs are constructed with an inflation rule instead of an extraction rule, thus avoiding sparse structures at higher recursion orders. GFiZPs can be classified as three types, i. e. $m=n$; $m>1$, $n=1$; and $m=1$, $n>1$. In each type, the trend of axial irradiance with various structural parameters can be readily tuned. Moreover, the ratio of widths between the two elementary bars in GFiZPs is considered as an additional parameter to engineer GFiZPs and its effect on axial irradiance was also studied using the twist plots. The GFiZP is anticipated to find more applications in focusing and imaging in soft-x rays and the THz band with versatile tailoring features.

References

[1] WANG S, ZHANG X. Terahertz tomographic imaging with a Fresnel lens[J]. Chinese Optics Letters, 2003, 1(1): 53-55.

[2] WANG Y, YUN W, JACOBSEN C. Achromatic Fresnel optics for wideband extreme-ultraviolet and X-ray imaging [J]. Nature, 2003, 424(6944): 50-53.

[3] CAO Q, JAHNS J. Modified Fresnel zone plates that produce sharp Gaussian focal spots[J]. Journal of the Optical Society of America A-Optics Image Science and Vision, 2003, 20(8): 1576-1581.

[4] SAAVEDRA G, FURLAN W D, MONSORIU J A. Fractal zone plates[J]. Optics Letters, 2003, 28(12): 971-973.

[5] DAVIS J A, RAMIREZ L, MARTÍN-ROMO J A R, et al. Focusing properties of fractal zone plates: experimental implementation with a liquid-crystal display[J]. Optics Letters, 2004, 29(12): 1321-1323.

[6] MONSORIU J A, SAAVEDRA G, FURLAN W D. Fractal zone plates with variable lacunarity[J]. Optics Express, 2004, 12(18): 4227-4234.

[7] DAI H T, WANG X, XU K S. Focusing properties of fractal zone plates with variable lacunarity: experimental studies based on liquid crystal on silicon[J]. Chinese Physics Letters, 2005, 22(11): 2851-2854.

[8] MUNOZ-PEREZO F M, FERRAND V, FURLAN W D, et al. Optical multi-trapping by Kinoform m-Bonacci lenses [J]. Optics Express, 2022, 30(19): 34378-34384.

[9] CANDELAS P, PEREZ-LOPEZ S, FUSTER J M. On the Design of Soret Zone Plates Based on Binary Sequences Using Directional Transducers[J]. Sensors, 2021, 21(18): 6086.

[10] XIA T, CHENG S B, YU W X, et al. Extended bifocal depth imaging with modified generalized composite kinoform Fibonacci lenses[J]. Optics and Laser Technology, 2022, 152: 108162.

(下转第 318 页)

[23] ARDILA L A P, POHL T. Ground-state properties of dipolar Bose polarons[J]. IOP Publishing, 2019(1).

[24] GUENTHER N E, MASSIGNAN P, LEWENSTEIN M, et al. Bose polarons at finite temperature and strong coupling[J]. Physical Review Letters, 2018, 120(5): 050405.

[25] ICHMOUKHAMEDOV T, TEMPERE J. Feynman path-integral treatment of the Bose polaron beyond the Fröhlich model[J]. Physical Review A, 2019, 100(4): 043605.

[26] FIELD B, LEVINSEN J, PARISH M M. Fate of the Bose polaron at finite temperature[J]. Physical Review A, 2020, 101(1): 013623.

[27] CHIN C, GRIMM R, JULIENNE P, et al. Feshbach resonances in ultracold gases[J]. Reviews of Modern Physics, 2008, 82(2): 1225-1286.

[28] YUTAKA T. Self-Trapping of an Electron by the acoustical mode of lattice vibration. I[J]. Progress of Theoretical Physics, 1961(1): 29-44.

[29] SUMI A, TOYOZAWA Y. Discontinuity in the polaron ground state[J]. Journal of the Physical Society of Japan, 1973, 35(1): 137-145.

[30] GENNES P G D. Effects of double exchange in magnetic crystals[J]. Physical Review, 1960, 118(1): 141-154.

[31] LI X, ZHU B, HE X, et al. Coherent heteronuclear spin dynamics in an ultracold spinor mixture[J]. Physical Review Letters, 2015, 114(25): 255301-255301.

[32] DEVREESE J T, ALEXANDROV A S. Fröehlich Polaron and Bipolaron: Recent developments[J]. Reports on Progress in Physics, 2009, 72(6): 066501.

[33] MITRA T K, CHATTERJEE A, MUKHOPADHYAY S. Polarons[J]. Physics Reports, 1987, 153(2-3): 91-207.

[34] HO, Tin-Lun. Spinor Bose condensates in optical traps[J]. Physical Review Letters, 1998, 81(4): 742-745.

[35] XU Z F, WANG D J, YOU L. Quantum spin mixing in a binary mixture of spin-1 atomic condensates[J]. Physical Review A, 2012, 86(1): 164-164.

[36] BOGOLYUBOV N N. On the theory of superfluidity[M]. 1971.

[37] KAWAGUCHI Y, UEDA M. Spinor Bose-Einstein condensates[J]. Physics Reports, 2012, 520(5): 253-381.

[38] FRÖHLICH H, PELZER H, ZIENAU S. XX. Properties of slow electrons in polar materials[J]. Philosophical Magazine, 2009, 41(314): 221-242.

[39] FEYNMAN R P. Statistical mechanics: A set of lectures [M]. 2018.

[40] LEE T D, LOW F E, PINES D. The motion of slow electrons in a polar crystal[J]. Physical Review, 1953, 90(2): 297-302.

[41] Van KEMPEN E G M, KOKKELMANS S J J M F, HEINZEN D J, et al. Interisotope determination of ultracold rubidium interactions from three high-precision experiments[J]. Physical Review Letters, 2002, 88(9): 93201-93201.

[42] PROVIDENCIA J D, RUIVO M D C, CÉLIA A de Sousa. The Hartree-Fock and generator coordinate methods in field theory. The polaron problem[J]. Annals of Physics, 1975, 91(2): 366-374.

[43] PEETERS F M, DEVREESE J T. Acoustical polaron in three dimensions: The ground-state energy and the self-trapping transition[J]. Phys Rev B Condens Matter, 1985, 32(6): 3515-3521.

■

(上接第 309 页)

[11] XIA T, CHENG S B, TAO S H. A general n-fractal aperiodic zone plate[J]. Journal of Modern Optics, 2019, 66(11): 1179-1189.

[12] LIU S, LIU X J, XIONG Y, et al. Multi-helix beams generated with binary helico-conical phase patterns[J]. Journal of the Optical Society of America A-Optics Image Science and Vision, 2023, 40(9): 1706-1713.

[13] LIU Y J, DAI H T, SUN X W, et al. Electrically switchable phase-type fractal zone plates and fractal photon sieves [J]. Optics Express, 2009, 17(15): 12418-12423 .

[14] DAI H T, LIU J H, SUN X C, et al. Programmable fractal zone plates (FraZPs) with foci finely tuned[J]. Optics Communications, 2008(22), 281: 5515-5519.

[15] FURLAN W D, SAAVEDRA G, MONSORIU J A. White light imaging with fractal zone plates[J]. Optics Letters 2007, 32(15): 2109-2111.

[16] BRUNO-ALFONSO A, REYES-GÓMEZ E, CAVALCANTI S B, Oliveria L E. Band edge states of the ⟨n⟩=0 gap of Fibonacci photonic lattices[J]. Physical Review A, 2008, 78(3): 035801.

[17] GELLERMANN W, KOHMOTO M, SUTHERLAND B. Localization of light waves in Fibonacci dielectric multilayers[J]. Physical Review Letters,1994, 72(5): 633-636.

[18] DAI H T, LIU Y J, SUN X W. The focusing property of the spiral Fibonacci zone plates[J]. 2012, Proceedings SPIE 8257, 82570T.

[19] GAO N, ZHANG Y C, XIE C Q. Circular Fibonacci gratings[J]. Applied Optics, 2011, 50(31): G142-G148.

[20] OH G Y, LEE M H. Band-structural and Fourier-spectral properties of one-dimensional generalized Fibonacci lattices [J]. Physical Review B, 1993, 48(17): 465-477.

■